Available online at www.sciencedirect.com

SCIENCE DIRECT

Nuclear Instruments and Methods in Physics Research B 241 (2005) 23–29

NIM B
Beam Interactions with Materials & Atoms

www.elsevier.com/locate/nimb

EUV emission from xenon in the 10–80 nm wavelength range using a compact ECR ion source

H. Merabet [a,*], S. Kondagari [a], R. Bruch [a], S. Fülling [a], S. Hahto [b], K.-L. Leung [b], J. Reijonen [b], A.L. Godunov [c], V.A. Schipakov [d]

[a] Department of Physics, University of Nevada Reno, Reno, NV 89557, USA
[b] Lawrence Berkeley National Laboratory, Berkeley, CA 94720, USA
[c] Department of Physics, Old Dominion University, Norfolk, VA 23529, USA
[d] Troitsk Institute for Innovation and Fusion Research, Troitsk 142092, Russia

Available online 9 November 2005

Abstract

In this work we have studied the generation of EUV light by a novel compact electron cyclotron resonance ion source (CECRIS). The EUV emission diagnostics of the ECR plasma was accomplished by means of a 1.5 m grazing incidence monochromator which was operated in a wavelength range of 4–90 nm under the condition of medium to high resolution to discriminate between spectra arising from different Xe^{q+} ($q = 2$–10) charge states. One of the major accomplishments of this study is assignment of numerous new optical transitions for xenon in the 10–80 nm range to create a database for further investigations. High resolution spectra were recorded in the 10–16 nm range confirming significant contributions from highly excited Xe^{10+} and Xe^{9+} ionic states. Major outcome of this work is that the Xe^{10+} ion emission with $\lambda = 13.4$ nm may occurs with such a simplified and compact ECR source. The EUV emission of this particular line is of great interest for lithography applications.
© 2005 Elsevier B.V. All rights reserved.

PACS: 32.30.−r; 32.30.Jc; 32.70.−n; 32.70.Fw

Keywords: EUV emission; Xenon atomic spectra; 13.4 nm; Plasma discharge; EUV lithography

1. Introduction

Potential extreme ultraviolet (EUV) light sources for lithography applications include laser produced plasmas as well as gas discharge ion sources [1]. While substantial progress has been

* Corresponding author. Address: Dhofar University, Sultanate of Oman. Tel.: +968 23 225 061x486; fax: +968 23 225 064.

E-mail addresses: hocine@physics.unr.edu, merabet@du.edu.om (H. Merabet).

0168-583X/$ - see front matter © 2005 Elsevier B.V. All rights reserved.
doi:10.1016/j.nimb.2005.07.233

made in the field of EUV spectrometry, there is still a strong need for new concepts for stable, efficient gas discharge based sources such as compact electron cyclotron resonance ion sources (CECRs) [2].

Lithography in the EUV range further extends optical lithography by using wavelength in the range of about 11–14 nm to shrink the size of printed features for integrated circuits manufacturing. These EUV systems currently under development utilize a wavelength of about 13.4 nm (13.4 nm roadmap). The reduced wavelength introduces several demanding challenges like (i) materials are strongly absorbent in the EUV region, (ii) systems require vacuum operation and (iii) EUV optical devices generally incorporate effective reflective surfaces based on multi-mirror technology [4]. Therefore EUV lithography (EUVL) requires technology advancement in the field of light source efficiency, mirror reflectivity, light source power, spectral purity, lifetime and stability [3].

To obtain reasonable intensities of highly charged xenon ions, a compact microwave plasma source was designed and developed by Leung et al. [4] at the Lawrence Berkeley National Laboratory (LBNL). The ECR plasma heating is accomplished using a 6.4 GHz microwave system, where a magnetic filed of 2.2 kG couples the microwaves efficiently to the plasma environment. This simplified CECR ion source employs a simple permanent magnetic ring structure to produce a dipole field. Xenon gas is of particular interest for the production of EUV light because it is inert and does not chemically react with other materials, which is highly desirable in the semiconductor industry. In this work we have measured and identified numerous new EUV radiative lines arising from xenon ions from charge state $q = 1$–10.

2. Results and discussion

In this study the EUV emission of the ECR plasma has been measured by a 1.5 m grazing incidence monochromator under the condition of medium and high wavelength resolution. The photons emitted in the source chamber enter a 500 mm long with 4 mm inner diameter glass capillary before passing through an entrance slit with a varying width (5 μm to 3 mm), depending of the desired resolution to be achieved. Then they strike a reflection grating at an angle of incidence of 88°. The 1.5 m radius concave grating with 600 grooves/mm and a blaze angle of 5° is positioned on a Rowland circle mounting. In this configuration the spectrometer covers a wavelength range of 4–90 nm. After reflection the photons pass through an exit slit also of a varying in width (5 μm to 3 mm) where they are then detected by a channeltron detector. With both slits set at 100 μm, a resolution of 0.1 nm at wavelength of about 30 nm is obtained, corresponding to a spectral resolution of $(\lambda/\Delta\lambda) \approx 304$. A PC controlled data acquisition system has been used to operate the apparatus and to record the data. A complete description of this experimental setup is given by Bruch and co-workers [5–7].

The emission spectra of Xe ions (from Xe^{+} to Xe^{10+}) have been calculated for the wavelength interval $\lambda = 10$–22 nm. The calculations have been carried out within relativistic Hartree–Fock (HF) approximation [8]. From 25 to 38 configurations including the ground state and single excited states were taken into account in the configuration interaction calculations for the each ion. Results of calculations have a good agreement with available experimental and theoretical data (see Table 1) [9,10]. Generally speaking for Xe^{1+} to Xe^{5+} configurations with 4d shell ($4d^9$) are important for Xe^{6+} and Xe^{7+} ions configurations with 4d and 5s*nl* or *nl* should play a major role. Moreover for Xe^{8+}–Xe^{10+} ions configurations with unfilled 4d shell have to be considered for the interpretation of the experimental data. Comparison of these theoretical results with experiment and previous work is shown in Table 1 for the 10–16 nm range. The HF theoretical results are given for initial and final configurations only. The detailed results will be presented elsewhere [11].

Fig. 1(a) illustrates a medium resolution xenon spectrum in the wavelength range 10–16 nm. Exhibited spectral peaks are labeled 1–28. A preliminary classification of this spectrum is summarized in Table 1. The dominating xenon lines are attributed to Xe^{7+}, Xe^{8+}, Xe^{9+} and/or Xe^{10+}. In addition, we have assigned some O^{3+}, O^{4+}, O^{5+} due to residual oxygen gas. In addition we have

Table 1
Line identification for the xenon background subtracted spectrum in the wavelength range 10–16 nm and comparison with theoretical predictions

Peak number	Relative intensity	Wavelength (nm) (this work)	Wavelength (nm) literature	Wavelength (nm) HF (this work)	State	Line identification	J–J
1	13.33	10.15	10.07		Xe IX[a]	$(4d^{10})^1S$–$(4d^95f)^3P$	0–1
				10.0729	Xe VII[g]	$4d^95s^26f$–$5s^2$	
2	19.38	10.283	10.282		Xe IX[a]	$(4d^{10})^1S$-$(4d^96p)^1P$	0–1
			10.381		Xe IX[a]	$(4d^{10})^1S$–$(4d^96p)^3P$	0–1
				10.3328	Xe IX[g]	$4d^96p$–$4d^{10}$	
3	40.88	10.716	10.724		Xe XI[c]	$(4d^8)^3F$–$(4d^95p)$	3–2
4	31.13	10.850	10.847		Xe XI[c]	$(4d^8)^1G$–$(4d^95p)$	4–3
			10.857		Xe XI[c]	$(4d^8)^3P$–$(4d^95p)$	2–2
				10.8807	XE XI[g]	$4d^95p6f$–$5p$	
5	30.13	10.952	10.940		Xe XI[c]	$(4d^8)^1D$–$(4d^95p)$	2–2
			10.948			$(4d^8)^3P$–$(4d^95p)$	1–2
6	17.85	11.112	11.113		Xe XI[c]	$(4d^8)^3F$–$(4d^74f)$	3–3
			11.126		Xe XI[c]	$(4d^8)^3F$–$(4d^74f)$	3–2
			11.129		Xe XI[c]	$(4d^8)^3P$–$(4d^74f)$	1–1
			11.139		Xe XI[c]	$(4d^8)^1G$–$(4d^74f)$	4–5
				11.1668	Xe VII	$4d^95s^25f$–$5s^2$	
7	39.87	11.520	11.563		Xe X[b]	$(4d^9)^2D$–$(4d^84f)$	3/2–3/2
			11.566			$(4d^9)^2D$–$(4d^84f)$	5/2–5/2
8	26.97	11.840	11.828		Xe XI[c]	$(4d^8)^3F$–$(4d^74f)$	4–3
				11.8284	Xe IV[g]	$4d^95p^26f$–$5p^2$	
				11.8398	Xe VI[g]	$4d^95p5f$–$5p$	
				11.8962	Xe VII[g]	$4d^95s^26p$–$5s^2$	
9	39.92	12.146	12.013		Xe IX[a]	$(4d^{10})^1S$–$(4d^96p)^1P$	0–1
10	34.43	12.350	12.3242		Xe VII[d]	$(5s^2)^1S$–$(d4f)^1P$	0–1
			12.3243		Xe VIII[e]	$(4d^{10}5s)^2S$–$(4d^95s4f)^2P^0$	1/2–1/2
			12.346		Xe VIII[e]	$(4d^{10}5s)^2S$–$(4d^95s4f)^2P^0$	1/2–3/2
11	29.75	13.004	13.04		N V[f]	$(2s)^2S$–$(11p)^2P^0$	1/2–3/2
			13.03		N VI[f]	$(2s)^2S$–$(11p)^2P^0$	1/2–3/2
			12.987		O VI[f]	$(1s^22p)^2P^0$–$(1s^24d)^2D$	3/2–5/2
				12.9598	XE IV[g]	$4d^95p^36f$–$5p^3$	
12	29.37	13.150	13.152		Xe XI[c]	$(4d^8)^1G$–$(4d^75p)$	4–3
			13.163		Xe XI[c]	$(4d^8)^1G$–$(4d^75p)$	2–2
			13.173		Xe XI[c]	$(4d^8)^1G$–$(4d^75p)$	4–5
				13.1950	Xe XI[g]	$4p^54d^9$–$4d^8$	
				13.1968	Xe X[g]	$4p^54d^{10}$–$4d^9$	
				13.1995	Xe X[g]	$4p^54d^95g$–$4d^85g$	
13	27.86	13.281	13.298		Xe XI[c]	$(4d^8)^3P$–$(4d^75p)$	1–2
					Xe III[g]	$(4d^8)^3P$–$(4d^75p)$	1–2
				13.2773	Xe V[g]	$4d^95p^3$–$4p^55p^3$	
				13.2829	Xe III[g]	$4p^55p^45g$–$4d^95p^45g$	
				13.2830	Xe IV[g]	$4d^95p^4$–$4p^55p^4$	

(*continued on next page*)

Table 1 (*continued*)

Peak number	Relative intensity	Wavelength (nm) (this work)	Wavelength (nm) literature	Wavelength (nm) HF (this work)	State	Line identification	J–J
14	23.89	13.396	13.404		Xe XI[c]	$(4d^8)^3F–(4d^75p)$	3–3
			13.409		Xe XI[c]	$(4d^8)^1D–(4d^75p)$	2–3
			13.412		N VII[c]	$(4d^8)^3F–(4d^74f)$	4–3
			13.387		N V[f]	$(2p)^2P^0–(3d)^2D$	3/2–5/2
			13.399		Xe XI[f]	$(2s)^2S–(8p)^2P^0$	1/2–3/2
				13.3724	Xe VII[g]	$4d^9\ 4f\ 5s^2–4p^54f\ 5s^2$	
				13.3726	Xe V[g]	$4d^9\ 4f\ 5p^2–4p^54f5p^2$	
				13.3740	Xe VI[g]	$4d^9\ 4f\ 5p–4p^54f5p$	
15	22.72	13.489	13.492		Xe XI[c]	$(4d^8)^1D–(4d^75p)$	2–1
			13.498		Xe XI[c]	$(4d^8)^3F–(4d^75p)$	3–4
			13.507		Xe XI[c]	$(4d^8)^3F–(4d^75p)$	4–5
			13.510		Xe XI[c]	$(4d^8)^3P–(4d^75p)$	2–3
			13.515		Xe XI[c]	$(4d^8)^3F–(4d^75p)$	3–4
				13.4436	Xe XI[g]	$4s\ 4d^85p–4s\ 4d^9$	
				13.4824	Xe XI[g]	$4s\ 4d^8\ 4f–4s\ 4d^9$	
				13.5247	Xe XI[g]	$4d^75p–4d^8$	
16	20.62	13.689	13.691		X XI[c]	$(4d^8)^1D–(4d^75p)$	1–3
				13.6301	Xe V[g]	$4d^95p^2\ 6p–5p^2$	
17	22.63	13.804	13.802		O V[f]	$(2s2p)^3P^0–(2s5d)^3D$	
			13.805		O V[f]	$(2s2p)^3P^0–(2s5d)^3D$	
			13.811		O V[f]	$(2s2p)^3P^0–(2s5d)^3D$	
				13.7516	Xe X[g]	$4d^8\ 4f–4d^9$	
				13.8508	Xe X[g]	$4s\ 4d^9\ 4f–4s\ 4d^{10}$	
18	25.65	13.921	13.917		Xe XI[c]	$(4d^8)^1G–(4d^75p)$	1–5
			13.902		O V[f]	$(2s^2)^1S–(2p(^3P^0_{3/2})3d)^1P^0$	0–1
				13.9100	Xe X[g]	$4p^54d^{10}–4p^54d^9\ 4f$	
19	23.59	14.094	14.103		Xe X[b]	$(4d^9)^2D–(4d^84f)$	3/2–1/2
			14.109		Xe X[b]	$(4d^9)^2D–(4d^84f)$	5/2–7/2
20	20.22	14.196	14.212		O V[f]	$(2s2p)^1P^0–(2s7d)^1D$	1–2
				14.2298	Xe IX[g]	$4d^9\ 4f–4d^{10}$	
21	10.56	14.459			Xe IX[a]	$(4d^{10})^1S–(4d^94f)^3D$	0–1
			14.361		Xe X[b]	$(4d^9)^2D–(4d^85p)$	5/2–3/2
			14.465		Xe X[b]	$(4d^9)^2D–(4d^85p)$	5/2–5/2
			14.477		O VIII[f]	$(3d)^2D–(9f)^2F^0$	5/2–7/2
			14.454	14.3982	Xe VIII[g]	$4d^9\ 4f\ 5s–5s$	
22	12.47	14.619	14.610		Xe X[b]	$(4d^9)^2D–(4d^84f)$	3/2–5/2
			14.614		Xe X[b]	$(4d^9)^2D–(4d^85p)$	5/2–7/2
				14.5827	Xe VII[g]	$4d^9\ 4f\ 5s^2–5s^2$	
				14.6634	Xe IV[g]	$4d^95p^3\ 6p–5p^3$	
23	12.22	14.71	14.700		Xe X[b]	$(4d^9)^2D–(4d^85p)$	3/2–3/2
			14.692		O V[f]	$(2s2p^2)^2P^0 – (2p(^2P^0_{3/2})4p)^1S$	1–0
						$4d^95p^45f–5p4$	
				14.7326	Xe III[g]	$4d^9\ 4f\ 5p–5p$	
				14.7488	Xe VI[g]		

Table 1 (*continued*)

Peak number	Relative intensity	Wavelength (nm) (this work)	Wavelength (nm) literature	Wavelength (nm) HF (this work)	State	Line identification	J–J
24	14.44	14.836	14.833		Xe X[b]	$(4d^9)^2D$–$(4d^85p)$	5/2–3/2
			14.835		Xe X[b]	$(4d^9)^2D$–$(4d^85p)$	3/2–5/2
			14.832		N V[f]	$(2p)^2P^0$–$(9s)^2S$	1/2–1/2
			14.838		N V[f]	$(2p)^2P^0$–$(9s)^2S$	3/2–1/2
				14.8005	Xe X[g]	$4s\,4d^95p$–$4s\,4d^{10}$	
				14.9083	Xe X[g]	$4d^85p$–$4d^9$	
25	9.78	14.997	15.027		Xe IX[a]	$(4d^{10})^1S$–$(4d^94f)^3P$	0–1
			15.008		Xe X[b]	$(4d^9)^2D$–$(4d^85p)$	3/2–3/2
			15.012		O VI[f]	$(1s^22s)^2S$–$(1s^23p)^2P^0$	1/2–3/2
			15.011		O VI[f]	$(1s^22s)^2S$–$(1s^23p)^2P^0$	1/2–1/2
					N V[f]	$(2p)^2P^0$–$(8d)^2P$	1/2–3/2
				14.9314	Xe V[g]	$4d^9\,4f\,5p^2$–$5p^2$	
26	21.64	15.593	15.591		O IV[f]	$(2s2p^2)^4P$–$(2p^23p)^4D^0$	5/2–7/2
27	17.20	15.797	15.802		N V[f]	$(2p)P^0$–$(6d)^2D$	1/2–3/2
			15.808		N V[f]	$(2p)P^0$–$(6d)^2D$	3/2-5/2
				15.8419	Xe III[g]	$4d^95p^4\,6p$–$5p^4$	
28	15.61	15.95	15.941		O V[f]	$(2p^2)^2P$–$(2p(^2P(^2P^0_{3/2})4d)^2D^0$	2–2
			15.940		Xe X[b]	$(4d^9)^2D$–$(4d^85p)$	3/2–3/2

[a] Callegari et al. [15].
[b] Churilov and Joshi [9].
[c] Kooijman [10].
[d] Churilov and Joshi [12].
[e] Churilov and Joshi [14].
[f] Kelly [13].
[g] HF calculations (this work).

found also contributions from N^{4+}, N^{5+} transitions due to the virtual leaks on the source. The dominant xenon lines arising from the excitation of Xe^{8+} ions stem from configurations $(4d^9nl)$ with $n = 4$, 5 and 6 decaying to the lower $(4d^{10})^1S$ state. The major contributions from Xe^{9+} photon decays would result from $(4d^8nl)$ excited states with $n = 4$ and 5 decaying to the $(4d^9)^2D$ lower state. Another important finding is the excitation of Xe^{10+} ions due to $(4d^7nl)$ configurations with $n = 4$ and 5 decaying to different lower states arising from $(4d^8)$ core. We further note that the most pronounced peak structure is centered at 10.716 nm may be attributed to $(4d^8)^3F$–$(4d^95d)$ decay. Another strong line occurs at 11.52 nm and could be assigned to $(4d^9)^2D$–$(4d^84f)$ fine structured transitions. The strongest contribution in the vicinity of 13.4 nm is the 13.396 nm peak which is dominated by Xe^{6+} (HF calculations, this work) and/or Xe^{10+} ionic states [12]. Fig. 1(b) exhibits a medium resolution section of xenon spectrum in the wavelength range of 16–22 nm. A resolution of about 270 was obtained for this spectrum using the 600 grooves/mm grating and about 23 lines were identified to originate form different ionization stages of Xe (Xe^{q+}, $q = 1$, 10) in this wavelength region. These data are available and will be published in the near future elsewhere [11].

We have also investigated the xenon spectrum in the higher wavelength region to gain more information about the different excitation and de-excitation processes. In Fig. 2(a) we have plotted a medium resolution xenon spectrum between 40–60 nm. It has been observed that the spectrum is dominated by xenon ions, however, residual contribution from oxygen and nitrogen ions are also present. In particular we have found that the most dominant xenon line structures arise from a variety of ions such as Xe^{2+}, Xe^{5+} Xe^{6+}, Xe^{8+} and Xe^{9+}. Additional observed line structures could

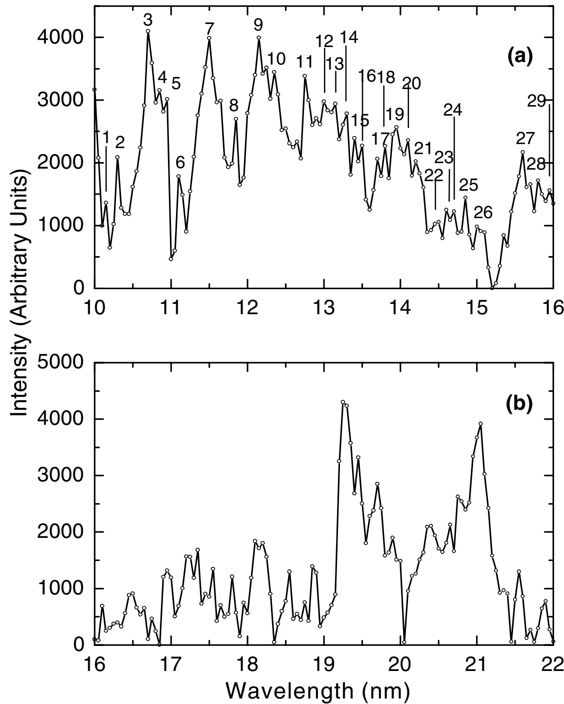

Fig. 1. Medium resolution xenon EUV spectrum between (a) 10 and 16 nm, (b) 16 and 22 nm. Continuous background was subtracted.

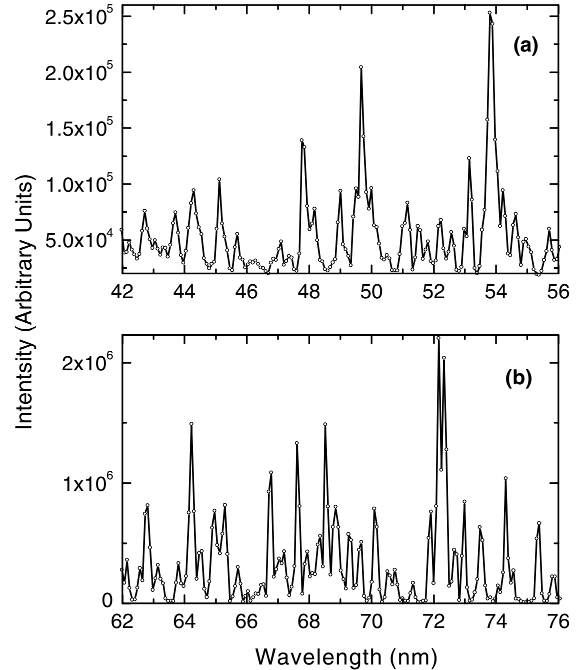

Fig. 2. Medium resolution xenon EUV spectrum between (a) 40 and 60 nm, (b) 60 and 80 nm. Continuous background was subtracted.

be assigned to N^{4+}, O^{2+}, O^{3+} and O^{5+} fine structure transitions. Interesting features observed in this spectrum are radiative decays among ($4d^9nl$) and ($4d^9nl'$) transitions for $n = 5$. Fig. 2(b) indicates the xenon spectral segment between 62 and 76 nm. This portion of the spectrum can be predominantly assigned to radiative transitions arising from Xe^{2+}, Xe^{3+}, Xe^{5+} and Xe^{6+} excited states. Moreover several peaks due to O^{2+}, O^{4+}, O^{7+}, N^{4+}, N^{6+} and N^{3+} have been identified. From the presented EUV data it is evident that the observed EUV xenon spectra are very rich and more detailed classification is presently under investigation.

In summary, we have presented a diagnostic of a novel compact electron cyclotron resonance ion source (CECRIS). Using EUV spectroscopy, we have identified numerous lines arising form Xe^{q+} ($q = 1$–10) in the 10–80 nm wavelength range. Furthermore, we have carried out emission spectra of xenon ions (Xe^{+} to Xe^{10+}) within a relativistic Hartree–Fock approximation. Results of calculations have a good agreement with our experiment as well as previous studies. Particular attention was devoted to the 13.4 nm roadmap region that has significant EUV lithography applications. We have shown in this study that the cost-effective and extremely compact light source can produce highly charged xenon EUV radiation in the vicinity of the 13 nm region. However we have found that the intensity and brightness of this source should be improved to match up to the high power requirements of lithography applications.

Acknowledgements

This project has been supported, in part, by Applied Photonics Worldwide (APW) Inc., Reno Nevada and the Nevada Business and Science Foundation (NBSF) Reno, Nevada. Dr. K.-L. Leung acknowledges support from International

SEMATECH under Contract No. 81FK and Department of Energy under Contract No. DE-AC03-76SF00098.

References

[1] K. Schriever, Microelectron. Eng. (2002) 61.
[2] R. Lebert, Microelectron. Eng. (2001) 57.
[3] Light for the next chip generators, Fraunhofer magazine, (2002) 2.
[4] K.-L. Leung, V. Bakshi, R. Bruch, S. Hahto, Q. Ji, S. Kondagari, H. Merabet, J. Reijonen, T. Schenkel, The generation of EUV light with a compact ECR source, Ion Beam Technology Group, Lawrence Berkeley National Laboratory.
[5] R. Bruch, E. Rauscher, S. Fülling, Encyc. Appl. Phys. 10 (1994) 437.
[6] M. Bailey, R. Bruch, E. Rauscher, S. Bliman, J. Phys. B 28 (1995) 2655.
[7] H. Merabet, M. Bailey, R. Bruch, J. Hanni, S. Bliman, D.V. Fursa, I. Bray, K. Bartschat, H.C. Tseng, C.D. Lin, Phys. Rev. A 64 (2001) 012712.
[8] R.D. Cowan, The Theory of Atomic Structure and Spectra, University of California Press, Berkeley, 1981.
[9] S.S. Churilov, Y.N. Joshi, Physica Scripta 65 (2002) 40.
[10] G. Kooijman, A laser plasma EUV source based on a supersonic xenon gas jet target, Thesis, FOM Institute, 2003.
[11] H. Merabet, R. Bruch, R. Bista, C. Schubert, S. Kondagari, S. Fülling, S. Hahto, K-L. Leung, J. Reijonen, A.L. Godunov, 2005, unpublished.
[12] S.S. Churilov, Y.N. Joshi, Phys. Scripta 62 (2000) 358.
[13] R.L. Kelly, Atomic and Ionic Spectrum Lines, 1982.
[14] S.S. Churilov, Y.N. Joshi, Phys. Scripta 65 (2002) 35.
[15] F. Callegari et al., J. Quant. Spectrosc. Radiat. Transf. 73 (2002) 13.